ISSN (Print) 1226-1750
ISSN (Online) 2233-6656
Journal of Magnetics 26(2), 166-174 (2021) https://doi.org/10.4283/JMAG.2021.26.2.166

Design of Concentrated Flux Synchronous Motor with Ferrite Magnet Considering Mechanical Stress at High Speed

Jeong-Jong Lee[1], Ki-Doek Lee[1], Hae-Joong Kim[2], and Myung-Hwan Yoon[1]*

[1]Intelligent Mechatronics Research Center, Korea Electronics Technology Institute
[2]Department of Electrical Engineering, Gyeongnam Namhae University

(Received 17 August 2020, Received in final form 13 June 2021, Accepted 15 June 2021)

This paper proposes a design of 90 kW concentrated flux synchronous motor (CFSM). A ferrite magnet is used because of low price compared to rare-earth materials and this spoke type structure of motor can be an alternative to the interior permanent magnet synchronous motor (IPMSM) using NdFeB. However, a greater size of ferrite magnet is required to achieve the same torque as NdFeB is used, because the residual induction of ferrite is approximately one third of NdFeB. Consequently, the spoke type structure is applied to improve the torque density. In the design process, methods of deciding the stack length, stator diameter, rotor diameter, and the number of poles and slots are suggested. Series turns per phase are determined by applying back-electromotive force-inductance map (EL map) in the initial design. A response surface method is applied for the optimization. Furthermore, a structural analysis is also conducted to confirm the safety at high speed. Finally, test of CFSM is conducted for the verification.

Keywords : concentrated flux, ferrite magnet, interior permanent magnet synchronous motor, mechanical stress

1. Introduction

Environment and energy are the critical problems of the industrial development. Demand for vehicles increases as an economy grows. Recently, electric vehicles (EVs) have attracted the attention and are widely used, because they have many advantages such as non-polluting, high energy efficiency, energy diversification, simple structural parts, and convenience of maintenance. An electric motor is one of key parts in the electric vehicles which require high efficiency and torque. Most of conventional motors use NdFeB because of high torque density, however the price of NdFeB is still expensive and unstable. This study proposes a design of 90 kW concentrated flux synchronous motor for a traction motor [1-4]. A ferrite magnet is used as an alternative material to NdFeB. The residual induction of ferrite magnet is approximately one third of that of NdFeB magnet. Therefore, a greater size of magnet is required to obtain the same performance which results in a spoke type rotor [5-12]. The design process of this motor is explained in detail as follows. First of all, the specification of this motor is presented and the size of motor is determined to increase the torque density which means the size minimization. The tendencies of efficiency, volume and torque density are analysed according to the outer diameter and the stack length with fixed torque per rotor volume (TRV). As a result, the longest stator outer diameter and the shortest stack length are the appropriate combination. The diameter ratio of stator and rotor is analysed [13]. The number of poles and slots are decided [14, 15]. Secondly, an initial model with determined poles, the ratio of stator and rotor, and the size is calculated by back-electromotive force (EMF)-inductance map (EL map). In case of synchronous motor, back-EMF and inductance have mainly effect on the characteristics of the motor. Therefore, ranges of the back-EMF and the inductance should be limited to obtain satisfactory characteristics. Parameters of the motor are presented on EL map with contour lines which are power, efficiency, current density and etc. The design criterion is easily determined by adjusting back-EMF and inductance, which is a reliable process. Parametric analysis is conducted to verify the result of EL map design process. In addition, thickness of teeth and yoke are optimized to increase the average torque and notch effect is checked to reduce the torque ripple. However, torque ripple, average torque and induced

*Corresponding author: Tel: +82-32-621-2845
Fax: +82-32-621-2855, e-mail: yoonmh@keti.re.kr

voltage are not satisfactory to the given specification. Therefore, response surface methodology (RSM) is applied to reduce torque ripple, induced voltage and increase efficiency [16, 17]. Eccentricity and slot opening are adjusted in RSM design process. As the spoke type is applied, magnets are placed in radial direction. Consequently, a space between magnet and shaft is limited where the mechanical stress can be concentrated. The shape of joint is investigated to secure the mechanical safety at high speed. The final model is obtained and the structural analysis is conducted at 6420 rpm which is 120 % of the maximum speed [18]. Demagnetization of PM is analysed by finite element method (FEM) on conditions of 150 % of the maximum line current and -40 degrees Celsius which results in no demagnetization. Thermal equivalent circuit of interior permanent magnet synchronous motor (IPMSM) is used to predict the temperature of the final model [19]. The model is manufactured and the test is conducted. As a result, the reliability of the motor design is verified with the test results.

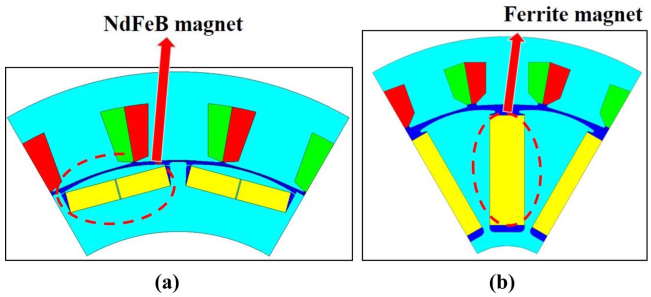

Fig. 1. (Color online) Shape of IPMSM: (a) NdFeB model, (b) Ferrite model

Table 1. CFSM specification.

Items	Unit	Vale
Stator outer diameter	mm	200
Rotor inner diameter	mm	45
Stack length	mm	200
DC link voltage	V	360
Power	kW	90
Maximum torque	Nm	170

2. Initial Design of Concentrated Flux Synchronous Motor

2.1. Feature of CFSM and specification

Concentrated flux synchronous motor (CFSM) is one of alternatives to the conventional motors using NdFeB [20-24]. As ferrite magnet is applied to CFSM, the greater size of magnet is necessary to perform the same power due to the lower residual induction of ferrite compared to NdFeB. Therefore, the arrangement of magnet is changed from the conventional IPMSM type where flux can be focused as shown in Fig. 1. Consequently, to maximize the size of magnets, the magnets occupy the space of rotor from the shaft to the outer rotor surface which means the space of rotor is fully used for the spoke type structure. The specification of the CFSM is presented in Table 1. The power of maximum rating is 90 kW where the torque is 170 Nm at 5200 rpm with 30 seconds operation. DC link voltage is 360 V and the motor is cooled by water. Current density at the maximum torque point is determined to be under 11 A/mm^2 refer to 30

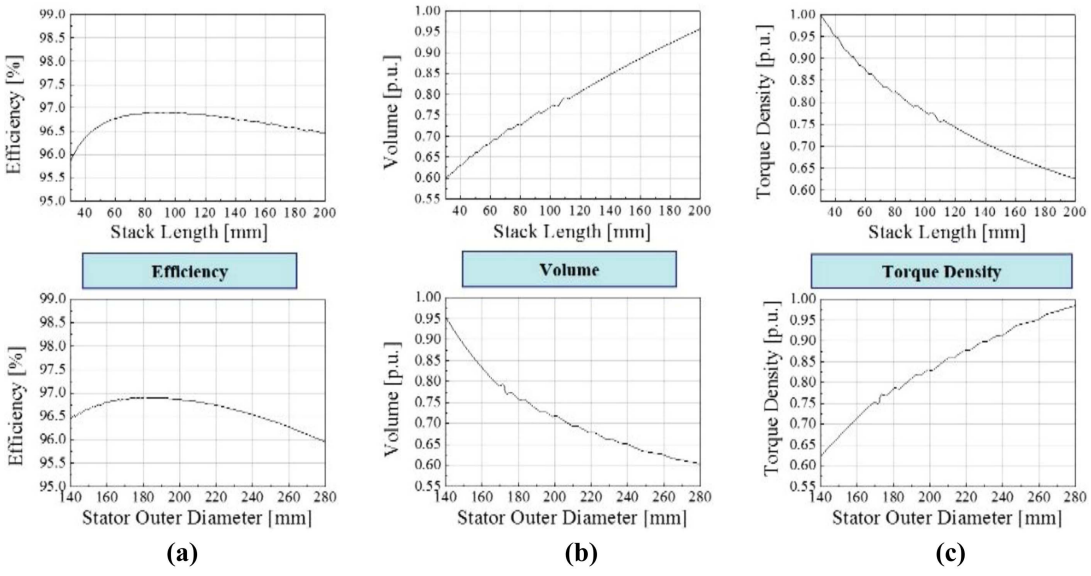

Fig. 2. (Color online) Tendency of efficiency, volume and torque density: (a) Efficiency, (b) Volume, (c) Torque density

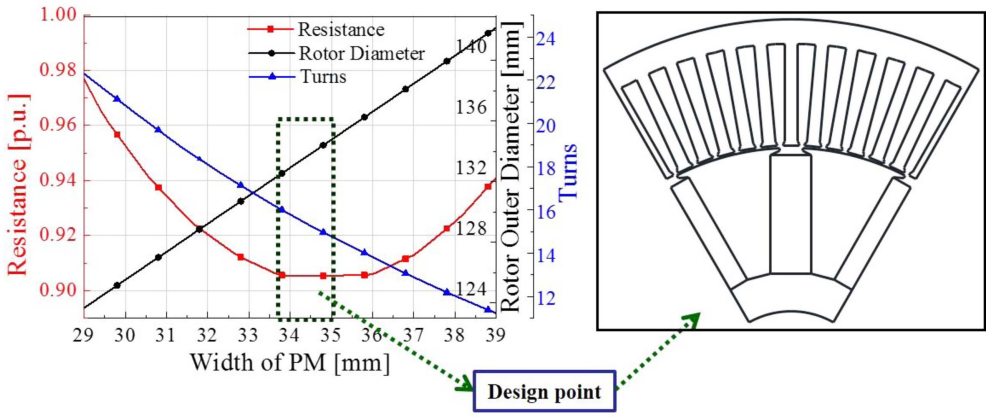

Fig. 3. (Color online) Characteristics according to PM width.

seconds operating.

2.2. Sizing of the motor

2.2.1. Stack length and stator outer diameter

Stator outer diameter and stack length are given. However, in order to minimize the size of motor, tendency of efficiency, torque density and volume according to the stack length and stator outer diameter is examined which are shown in Fig. 2. The torque density increases as the diameter increases with fixed TRV, consequently greater stator outer diameter and shorter stack length are advantageous to minimize the size.

2.2.2. Ratio of stator and rotor diameter

As the magnet is designed perpendicular to the air-gap for the ferrite model shown in the Fig. 1, a rotor diameter is directly relevant to the magnet width. Fig. 3 presents the characteristics according to PM width where the stator outer diameter is fixed and the same back-EMF is performed on no-load condition. This result is applied by lumped parameter and the design point is decided where the smallest resistance is obtained. At continuous zone, the copper loss is important factor for the efficiency, therefore the appropriate turns, rotor diameter and turns are determined.

2.2.3. Determination of poles and slots

Selecting the combination of poles and slots are the most important step in design of motors. The combination of poles and slots affects the torque and vibration [25-27]. The fractional slot concentrated winding is not used for the traction motor because of the critical vibration problem, therefore distributed winding pole slot combination is selected. As the number of poles increases, the thickness of stator yoke can decrease which can reduce the size of motor. However, as the number of slots increases, the thickness of teeth becomes thinner but there is a limit of the thinnest thickness due to the manufacture technology. The maximum of poles is decided by the speed of the motor and carrier frequency of the inverter which is 12 in this specification. The winding factor of pole and slot combination is presented in the Table 2. The value of 1st winding factor should be high because it is related to the torque of the motor, but other values affect torque ripple and vibration which are harmful to the motor. 36 slots and 72 slots are appropriate number of slots but it is difficult to manufacture 72 slots which are too thin.

Table 2. Pole and slot combination.

Pole / Slot	1st winding factor	5th winding factor	7th winding factor
12 / 18	0.866	0.866	0.866
12 / 36	1	1	1
12 / 72	0.966	0.259	0.259

2.3. Initial model

2.3.1. Initial model

12 pole and 36 slot model is determined to be an initial model considering the winding factor, manufacture technology and the reliability of control. Specification of the model is presented in Table 3. Efficiency, current and voltage of the model are checked by the E-L Map. Back-

Table 3. Specification of initial model.

Items	Unit	Vale
Pole / Slot	-	12 / 36
Stator outer diameter	mm	200
Air-gap / Stack length	mm	0.5 / 167
Series turns per phase	mm	16
Material of magnet	Br=0.38@100°C	Ferrite (NMF-12G)

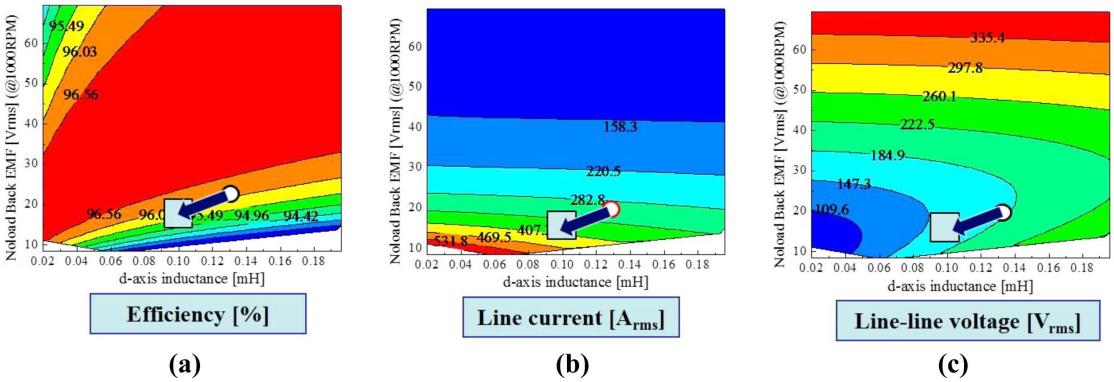

Fig. 4. (Color online) The result of E-L map: (a) Efficiency, (b) Line current, (c) Line-line voltage

EMF and inductance are the main factors which affect the characteristics of the synchronous motor. Consequently, ranges of back-EMF and inductance should be limited to obtain a desirable characteristics and the design target can be easily get by adjusting the two parameters. The result of E-L Map is shown in Fig. 4. The status of initial model is presented as circles on the graphs and contour lines are shown for the reference values. The squares are the target points satisfying the required specification. As the back-EMF is proportional to series turns per phase and the inductance is proportional to the square value of the turns with the same resistance, the fewer turns of initial model are required to move the circle to the square which represent the initial point and the target point respectively. Therefore, series turns per phase is changed from 16turns to 14 turns.

2.3.2. Design of notch

Torque ripple and induced voltage exceeding the input voltage are caused by harmonic components of the current and back-EMF. The torque ripple has a harmful influence on vibration, noise and the induced voltage. The induced voltage exceeding the input voltage results in the insufficient voltage. Accordingly, the current is distorted and decreased which causes the decrease in the torque. Therefore, the sinusoidal wave forms of current and back-EMF are necessary for the satisfactory performance of the motor. A notch is one of methods reducing the torque ripple and applied to the motor [21, 22]. Three models are compared which are no notch, 1 mm notch width and 2 mm notch width models. Applying 2 mm notch is appropriate because the value of torque ripple is the minimum and the induced voltage can be also reduced with the same average torque compared to other models as shown in Fig. 5.

2.3.3. Design of teeth yoke

Different widths of yoke and teeth are compared with the same slot area and current condition. That is, the same fill factor and current density are applied. The average torque according to the width is examined. As a result, 8.6 mm width of yoke model performs the greatest torque where the saturation on load condition is reflected as presented in Fig. 5.

2.3.4. Parametric analysis

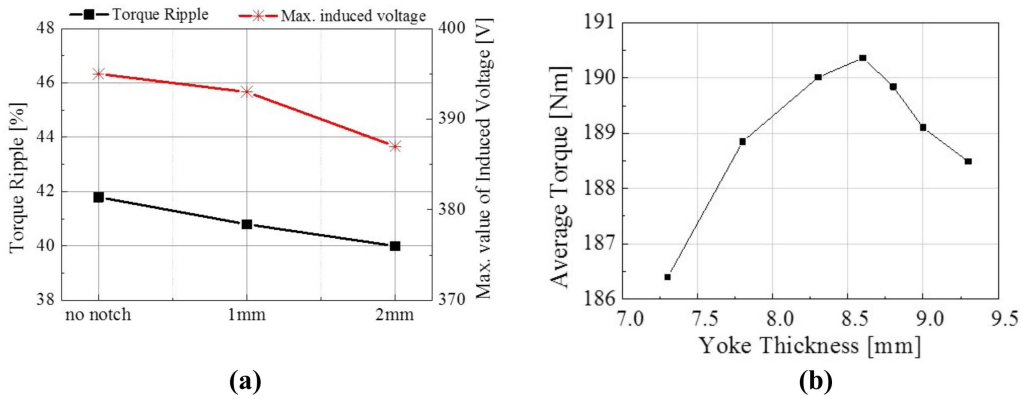

Fig. 5. (Color online) Tendency according to notch and yoke thickness: (a) Notch, (b) Yoke thickness

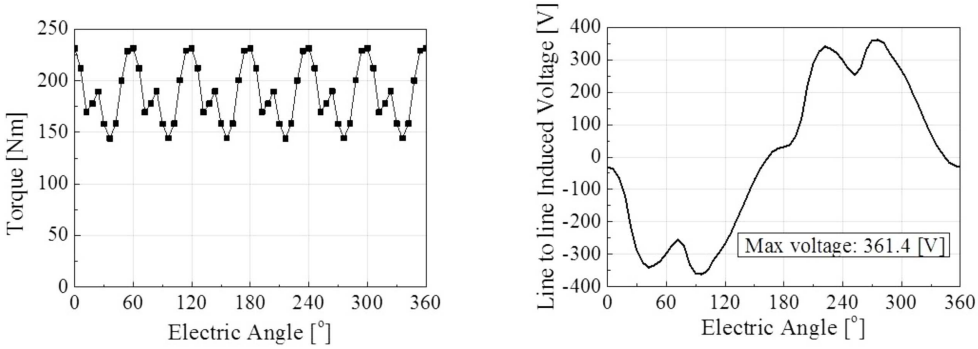

Fig. 6. Waveforms of torque and induced voltage: (a) Torque, (b) Induced voltage

As dimensions are decided, an initial model is modified and parameters of the model are analysed. Torque, torque ripple, induced voltage and efficiency map are obtained. As a result, the maximum torque is satisfying the target, however the torque ripple is approximately 46 % which is relatively high. Furthermore, the maximum value of induced voltage is over an input voltage therefore the induced voltage is required to be reduced. Waveforms of torque and line to line induced voltage are obtained by $380A_{rms}$ of current and 30° of current angle at 5200 rpm are presented in Fig. 6.

3. Optimization

As mentioned above, torque, torque ripple, and induced voltage of the initial model are obtained, however torque ripple and induced voltage are not satisfied yet. Therefore, RSM is applied to find the optimum model where the performances of the model are satisfied. The method explores the relationships between several explanatory variables and one or more response variables. Values or ranges satisfying torque characteristic are calculated by RSM. As an efficiency is the most important factor for the traction motor, maximization of efficiency, minimization of torque ripple and induced voltage are set to be the objective function. Performing torque over the target which is 170 Nm torque is the constraint condition. Slot opening of stator and eccentricity are determined to be design factors which are effective parameters to minimize torque ripple and induced voltage. The eccentricity which is defined in the paper as shown in Fig. 7. makes uneven air-gap length and this causes decrease in both torque and torque ripple. Therefore, an appropriate value is required for the design. Then, the optimal solution is obtained as shown in Table 4 respectively. Additional FEM is conducted to confirm the RSM result and compared in Table 4. The range of slot opening is from 0 mm to 2 mm and eccentricity is from 0 mm to 28 mm. All the weighting factors are 1 and Table 4 presents the value of objective function. As a result, the torque ripple and the maximum value of induced voltage are reduced and the efficiency increased with 28 mm eccentricity.

Table 4. RSM and FEM results.

Items	Initial model	Optimized model	FEM
Slot opening	2	2	2
Eccentricity	0	28	28
f_{net}	311.5 ripple : 46.3 voltage : 360.7 efficiency : 95.5	283.7 ripple : 18.5 voltage : 360.8 efficiency : 95.6	281.4 ripple : 17.3 voltage : 359.8 efficiency : 95.7

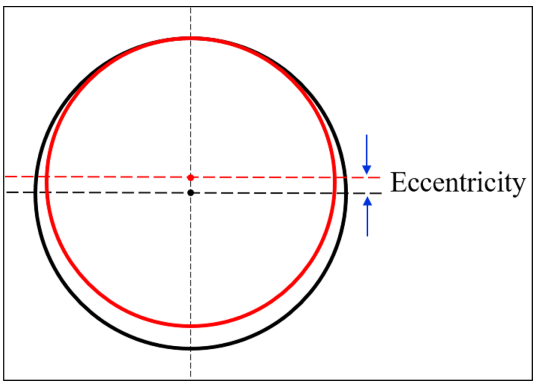

Fig. 7. (Color online) Definition of eccentricity.

4. Structural Analysis, Demagnetization, and Thermal Analysis

4.1. Structural analysis

A structural analysis is conducted for examining mechanical stiffness of the optimized model [20]. In this motor design, non-magnetic material is applied between the

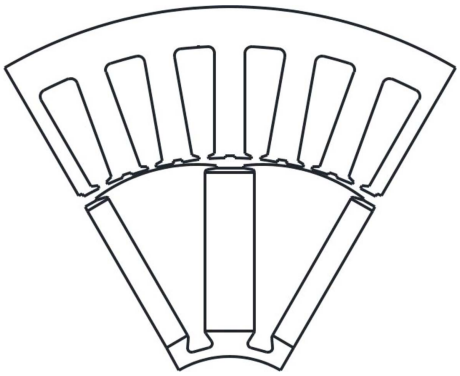

Fig. 8. Two pole model of final model.

magnet and shaft to prevent the leakage flux. The maximum stress is expected to occur at joint where core and non-magnetic material are connected, because all the centrifugal forces on the rotor components are in radial direction and the joint can hold the components against the forces. As the magnet is designed perpendicular to the air-gap for CFSM as shown in the Fig. 1, all the components can escape in radial direction without the joint. Therefore, the shapes of joint are examined to satisfy the allowable stress. As rotor dimensions except the joint are determined, the resultant force is constant and the peak stress can be reduced by wide spread distribution. For example, a greater radius of fillet in the joint and the bigger size of the joint can avoid the concentration of stress. However, the size of the joint can be designed within the given space of non-magnetic material. The shape of joint is decided and the final model is presented in Fig. 8. In addition, a filler is filled in the space between two cores and above the magnet. ANSYS, which is FEM tool for the structural analysis, is used in this paper. Boundary conditions for the analysis are presented in Fig. 9 and the speed of analysis is 6420RPM which is 1.2 times the maximum speed of the specification. Most of boundary conditions are considered as frictionless which is an extreme condition where a friction is neglected. According to the FEM result, the maximum stress occurs at non-magnetic material as expected. The yield point of core is 440 MPa and non-magnetic material is 450 MPa. The result of analysis is presented in Fig. 8 and the maximum stress is 191.6 MPa on the non-magnetic material. In other word, the safety factor is 2.35 which is an appropriate value to use where 2 is the general value of motor designs for the safety.

4.2. Demagnetization

NMF-12G is ferrite material used for the permanent magnet and can be demagnetized easily as temperature drops. Therefore, demagnetization should be checked in the extreme condition. In the paper, demagnetization of PM is analysed by FEM on conditions of 150 % of the maximum line current and -40 degrees Celsius. As shown in Fig. 10, B-H curves according to the temperature are shown and flux linkages on no-load condition are analysed

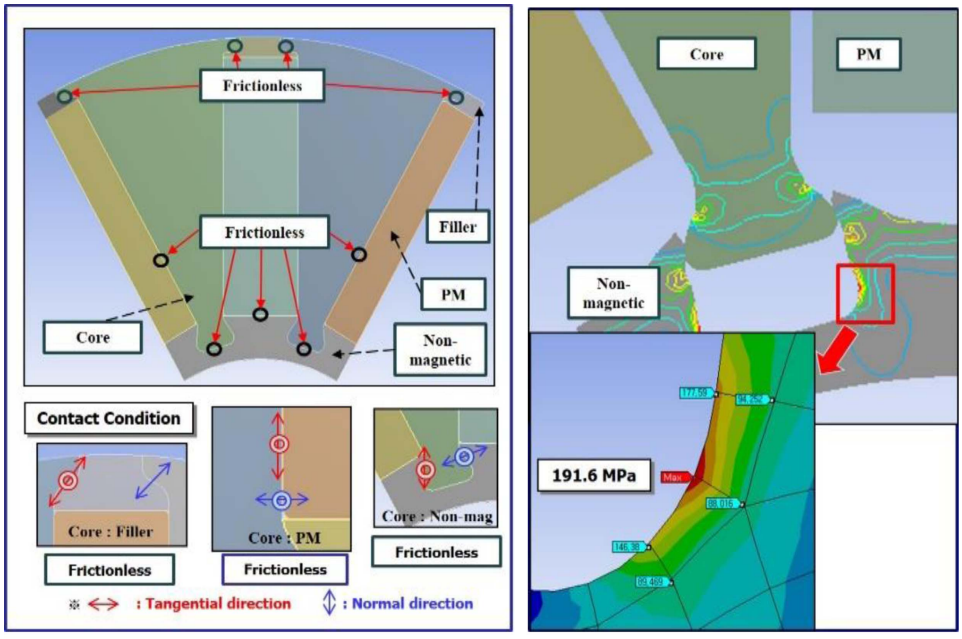

(a) **(b)**

Fig. 9. (Color online) Boundary conditions and result of structural analysis: (a) Boundary conditions, (b) Result of structural analysis

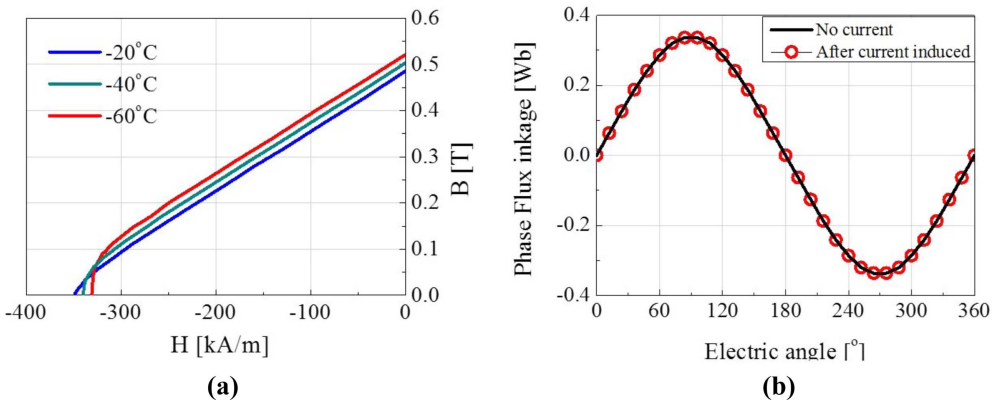

Fig. 10. (Color online) B-H curve and flux linkage: (a) B-H curve, (b) Flux linkage

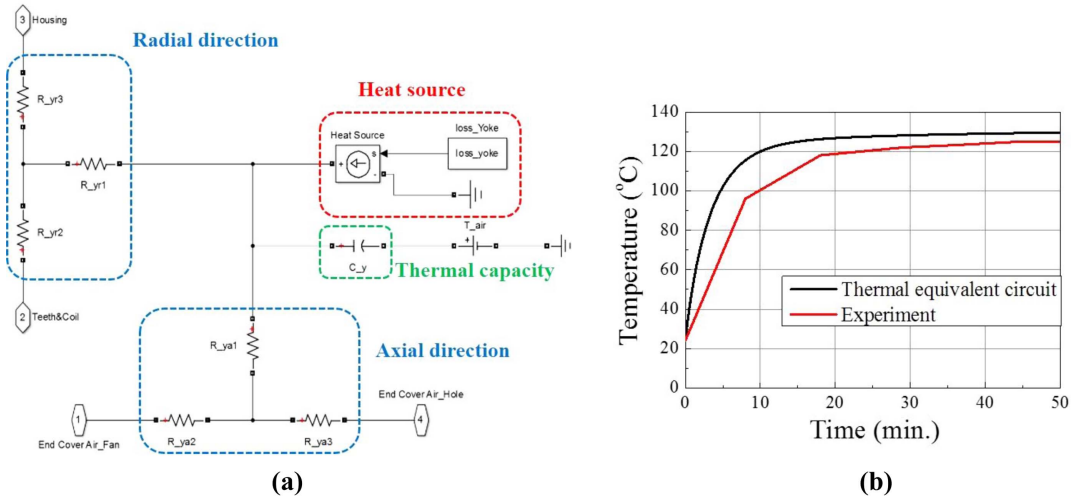

Fig. 11. (Color online) Thermal equivalent circuit and results: (a) Circuit, (b) Results comparison of thermal equivalent circuit and thermal test

before and after the current is induced. As a result, the same values are obtained where the magnet is not demagnetized.

4.3. Thermal analysis

Thermal equivalent circuit of IPMSM is used to predict the temperature of the final model. In the motor operation, copper loss, core loss and eddy current loss in the permanent magnet are generated. These losses are reflected as source and the thermal resistances are calculated on the basis of dimensional information and the constant thermal coefficient. The basic configuration of thermal equivalent

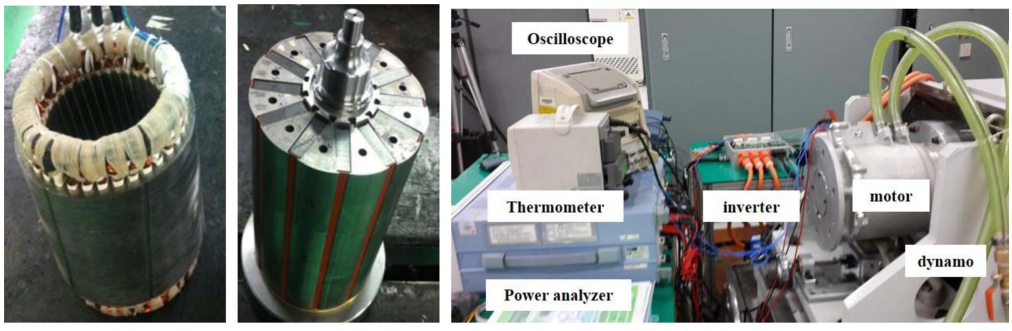

Fig. 12. (Color online) Manufactured model test configuration: (a) Stator, (b) Rotor, (c) Test configuration

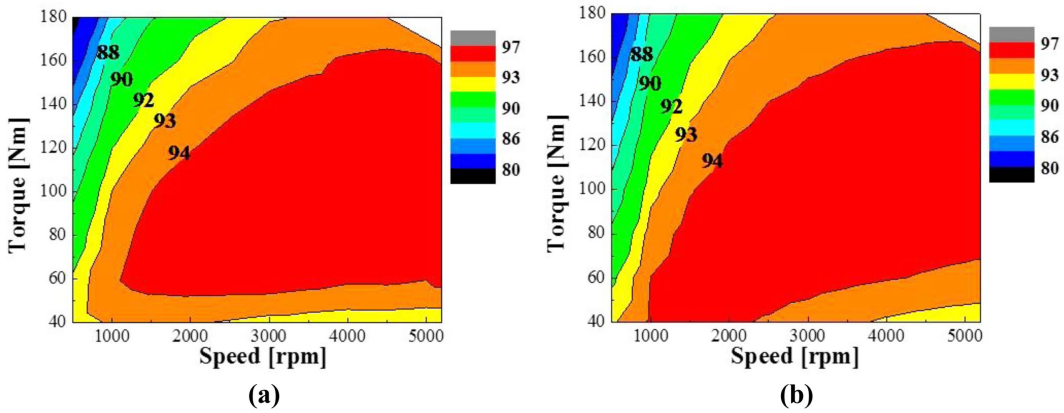

Fig. 13. (Color online) Efficiency map: (a) Test result, (b) FEM result

circuit is shown in Fig. 11. Results of thermal equivalent circuit are compared to the thermal test for the verification as presented in Fig. 11. As N class of insulation is used in the model, the maximum allowable temperature is 200 degrees Celsius. According to the results of the experiment and FEM, the temperature of end coil converges in 135 degree Celsius. Therefore, there is no thermal problem with this motor.

5. Result

Designing methods of CFSM are presented above and the final model is necessary to be checked for the satisfactory performance. The final model is presented in Fig. 8 and characteristic analysis of the model is conducted. According to the FEM results, 170 Nm of torque satisfies the target. Furthermore, the model is manufactured as presented in Fig. 12 and the test is conducted for the verification. The test configuration is composed as shown in Fig. 12. Efficiency maps obtained by FEM and the test are compared in Fig. 13. Consequently, the suggested method in this paper is verified.

6. Conclusion

In this paper, the design of 90 kW CFSM for the traction application is proposed. A spoke type motor is necessary for the increase in torque density. According to this design process, the spoke type motor can be designed with ferrite magnet. The spoke type motor using a ferrite magnet which can be substituted for the conventional motor using NdFeB where the price of NdFeB is 8 times higher than ferrite recently and it is always affected by Chinese policy on rare earth supply. The spoke type motor is designed with a ferrite magnet. Methods of sizing, determining the ratio of stator and rotor, and deciding the number of poles and slots are suggested. Series turns per phase are determined by applying E-L map to the initial design. RSM is applied for the optimization. Thermal, demagnetization and structural analysis are also conducted. Especially, the safety factor is the most important consideration for the traction motor where the high speed and high torque are required. Test is conducted for the verification and the suggested design method will be useful for designing motors of high speed and high torque.

Acknowledgement

This work was supported by Korea Institute of Energy Technology Evaluation and Planning (KETEP) grant funded by the Korea government (MOTIE) (20192010106780, A Construction and Operation of Open Platform for Next-Generation Super Premium Efficiency (IE4) Motors).

References

[1] Y. H. Jung, M. S. Lim, M. H. Yoon, J. S. Jeong, and J. P. Hong, IEEE Trans. Energy Convers. **33**, 333 (2018).
[2] J. H. Park, K. T. Jung, Y. H. Jung, M. S. Lim, M. H. Yoon, and J. P. Hong, IEEE Trans. Ind. Appl. **55**, 3534 (2019).
[3] M. S. Lim, S. H. Chai, J. S. Yang, and J. P. Hong, IEEE Trans. Ind. Electron. **62**, 7287 (2015).
[4] J. H. Lee and B. Kwon, IEEE Trans. Magn. **49**, 2205 (2013).
[5] H. J. Kim, D. Y. Kim, and J. P. Hong, IEEE Trans. Magn. **50**, 8206704 (2014).
[6] J. Li and K. Wang, IEEE Trans. Mechatron. **24**, 2182 (2019).
[7] Q. Chen, G. Xu, G. Liu, F. Zhai, and S. Eduku, IEEE Trans. Ind. Electron. **67**, 9613 (2020).
[8] S. G. Lee, J. B, and W. H. Kim, IEEE Trans. Appl. Supercond. **30**, 5205706 (2020).

[9] M. Si, X. Y. Yang, S. W. Zhao, and S. Gong, IET Electr. Power Appl. **10**, 571 (2016) .
[10] M. M. Rahman, K. T. Kim, and J. Hur, IEEE Trans. Magn. **49**, 2397 (2013).
[11] K. D. Lee, J. Lee, and H. W. Lee, IEEE Trans. Magn. **51**, 8204304 (2015).
[12] K. S. Kim, M. R. Park, H. J. Kim, S. H. Chai, and J. P. Hong, IEEE Trans. Magn. **52**, 8101804 (2016).
[13] W. Chu, Z. Zhu, and Y. Shen, IET Electr. Syst. Transp. **3**, 41 (2013).
[14] M. Valavi, A. Nysveen, R. Nilssen, R. D. Lorenz, and T. Rølvåg, IEEE Trans. Magn. **50**, 8700111 (2014).
[15] H. J. Kim, D. J. Kim, and J. P. Hong, IEEE Trans. Magn. **50**, 7019504 (2014).
[16] Y. Yokoi and T. Higuchi, IEEE Trans. Magn. **51**, 8202911 (2015).
[17] B. H. Lee, J. P. Hong, and J. H. Lee, IEEE Trans. Magn. **48**, 863 (2012).
[18] J. W. Jung, B. H. Lee, D. J. Kim, J. P. Hong, J. Y. Kim, S. M. Jeon, and D. H. Song, IEEE Trans. Magn. **48**, 911 (2012).
[19] N. Bracikowski, M. Hecquet, P. Brochet, and S. V. Shirinskii, IEEE Trans. Magn. **59**, 2426 (2012).
[20] S. I. Kim, S. Park, T. Park, J. Cho, W. Kim, and S. Lim, IEEE Trans. Ind. Electron. **61**, 5763 (2014).
[21] M. M. Rahman, K. T. Kim, and J. Hur, IEEE Trans. Magn. **50**, 7021404 (2014).
[22] L. Hao, M. Lin, D. Xu, N. Li, and W. Zhang, IEEE Trans. Magn. **51**, 8208304 (2015).
[23] Y. U. Park, J. H. Cho, and D. K. Kim, IEEE Trans. Ind. Appl. **51**, 4455 (2015).
[24] S. Ramarathnam, A. K. Mohammed, B. Bilgin, A. Sathyan, H. Dadkhah, and Ali. Emadi, IEEE Trans. Transp. Electrif. **1**, 255 (2015).
[25] M. R. Park, J. W. Jung, D. Y. Kim, J. P. Hong, and M. S. Lim, IEEE Trans. Ind. Appl. **55**, 1351 (2019).
[26] T. Sun, J. M. Kim, G. H. Lee, J. P. Hong, and M. R. Choi, IEEE Trans. Magn. **47**, 1038 (2011).
[27] D. Y. Kim, M. R. Park, J. H. Sim, and J. P. Hong, IEEE Trans. Mechatron. **22**, 1554 (2017).